The Fast Response of the Tropical Circulation to CO_2 Forcing

ELINA PLESCA, STEFAN A. BUEHLER, AND VERENA GRÜTZUN[a]

Meteorological Institute, Center for Earth System Research and Sustainability, University of Hamburg, Hamburg, Germany

(Manuscript received 15 February 2018, in final form 31 August 2018)

ABSTRACT

Atmosphere-only CMIP5 idealized climate experiments with quadrupling of atmospheric CO_2 are analyzed to understand the fast response of the tropical overturning circulation to this forcing and the main mechanism of this response. A new metric for the circulation, based on pressure velocity in the subsidence regions, is defined, taking advantage of the dynamical stability of these regions and their reduced sensitivity to the GCM's cloud and precipitation parameterization schemes. This definition permits us to decompose the circulation change into a sum of relative changes in subsidence area, static stability, and heating rate. A comparative analysis of aqua- and Earth-like planet experiments reveals the effect of the land–sea contrast on the total change in circulation. On average, under the influence of CO_2 increase without surface warming, the atmosphere radiatively cools less, and this drives the 3%–4% slowdown of the tropical circulation. Even in an Earth-like planet setup, the circulation weakening is dominated by the radiatively driven changes in the subsidence regions over the oceans. However, the land–sea differential heating contributes to the vertical pattern of the circulation weakening by driving the vertical expansion of the tropics. It is further found that the surface warming would, independently of the CO_2 effect, lead to up to a 12% slowdown in circulation, dominated by the enhancement of the static stability in the upper troposphere. The two mechanisms identified above combine in the coupled experiment with abrupt quadrupling, causing a circulation slowdown (focused in the upper troposphere) of up to 18%. Here, the independent effect of CO_2 has a considerable impact only at time scales less than one year, being overtaken quickly by the impact of surface warming.

1. Introduction

The latest investigations based on phase 5 of the Coupled Model Intercomparison Project (CMIP5; see Taylor et al. 2012) general circulation models (GCMs) show a consensus on the weakening of the tropical atmospheric circulation in response to global climate change (Held and Soden 2006; Vecchi and Soden 2007; Bony et al. 2013; Shepherd 2014; Kociuba and Power 2015). One would expect that both the increase in CO_2 itself and the subsequent climate system feedbacks, such as surface heating, play a role in the circulation slowdown, but their relative contributions are still unclear.

Most recent studies show that the increase in surface temperature, which is one of the most robust and important responses of the climate system to CO_2 increase, dominates and causes a decrease in the circulation intensity by enhancing the atmospheric stability of the lower troposphere (Vecchi and Soden 2007; He and Soden 2015). At the same time, Zelinka and Hartmann (2010) and Bony et al. (2013) argue that even in the absence of surface temperature increase, the tropical circulation will weaken if CO_2 concentration rises. This response relates to the radiative effect of CO_2 on the atmospheric cooling rate, as the latter weakens and therefore dampens the vertical atmospheric motion. In addition, there is insufficient certainty on the circulation's natural variability (Power and Kociuba 2011; Kociuba and Power 2015; Plesca et al. 2018), which may mask the anthropogenically induced weakening. The regional aspects of climate change introduce further uncertainty in our assessment of the circulation change: Ma and Xie (2013) argue that a large part of the intermodel spread in the tropical overturning circulation change is driven by the patterns in sea surface temperature change;

Supplemental information related to this paper is available at the Journals Online website: https://doi.org/10.1175/JCLI-D-18-0086.s1.

[a] Deceased.

Corresponding author: Elina Plesca, elina.plesca@uni-hamburg.de

DOI: 10.1175/JCLI-D-18-0086.1

Li and Ting (2017) and Gaetani et al. (2017) suggest, on the example of the Asian and West African monsoons, respectively, that at regional scales, the circulation actually strengthens under CO_2 forcing.

Here, we investigate the independent direct effect of CO_2 increase on the tropical overturning circulation, referred to also as the fast response of the circulation. Within this work, we use the term "fast response to CO_2" as a synonym to "direct effect of CO_2" considering that in an idealized coupled climate experiment that allows the sudden increase in concentration, the atmosphere would respond first to this change and only later to the subsequent surface warming and other climate feedbacks induced by the greenhouse effect of the additional CO_2. We develop a metric for the circulation intensity that allows the quantification of this CO_2 radiative effect on the total change in tropical circulation and the detection of the mechanism driving the change.

To separate the effect of CO_2 increase on the tropical circulation intensity from the effect of the surface warming, we make use of the CMIP5 tiered idealized climate experiments suite. First, we analyze the changes detected in climate experiments that feature quadrupled atmospheric CO_2 concentration with respect to a control climate state but with no subsequent surface warming (sea surface temperature and sea ice are prescribed to the control climate state). Further, we account for another phenomenon that affects the atmospheric circulation: the differential heating of land and ocean surfaces, as it acts as an additional forcing both at regional and global scales. For this, we begin by investigating the simple idealized case of the CMIP5 aquaplanets, which have no axial tilting, therefore, no seasons and zonal asymmetries in surface boundary conditions (Medeiros et al. 2015). Then we compare these results with the results obtained from the Atmospheric Model Intercomparison Project (AMIP; see Taylor et al. 2012) experiments. These experiments are set up on an Earth-like planet, but the climate system is limited to the atmosphere only, with sea temperature and sea ice being prescribed to modern patterns. Therefore, by comparing the two sets of experiments (without and with landmass and orography), we determine whether it is the land–sea contrast or the radiative response of the atmosphere that dominates the changes in atmospheric circulation.

It is common to investigate the tropical overturning circulation through the prism of both the convective and the subsiding regions in the atmosphere. Most metrics for the intensity of the circulation are based on the dynamics in the convective regions, on the difference between the convecting and subsiding regions for a certain parameter (e.g., mean sea level pressure, vertical velocity), and/or on the tropical precipitation patterns (e.g., Bony et al. 2013; Ma and Xie 2013; He and Soden 2015). However, Rybka and Tost (2014), Shepherd (2014), Su et al. (2014), and Merlis (2015) suggest that the cloud, precipitation, and convection parameterizations cause most of the uncertainty in the GCM simulation of atmospheric circulation. The new metric introduced here considers the vertical pressure velocity ω exclusively in the tropical subsidence regions and, therefore, reduces the impact of the abovementioned uncertainty on the results. The added value of our metric is that it gives the opportunity to decompose the relative change in circulation into a sum of relative changes in atmospheric cooling rate, stratification, and subsidence area. This decomposition allows us to clearly quantify the fast response of the circulation to CO_2 increase, as well as to determine the main drivers of this response and their relative roles. Such an approach allows for a better understanding of the mechanisms affecting this change and complements previous studies that addressed the direct individual impact of CO_2 on the atmospheric circulation (Bony et al. 2013; He and Soden 2015). Supplementary to this, we investigate the changes from the perspective of atmospheric profiles, which bring additional insight into the vertical spatial changes of the tropical overturning circulation.

As mentioned above, in a realistic climate system, the CO_2 concentration rise and surface warming have a combined effect on the atmospheric circulation. To put this study in such a realistic context, we start by determining the independent role of the surface temperature rise on the circulation intensity. Using the same approach as for the investigation of the increased CO_2 impact, we analyze two CMIP5 idealized climate experiments that maintain the CO_2 concentration but uniformly increase the sea surface temperature by 4 K. Consequently, the two detected responses (to CO_2 forcing and to temperature increase) are independent of each other and reveal the mechanisms driving each of them. In the broader context of a coupled climate system, these results allow us to determine the importance and the time extent of the responses. In this regard, we examine the idealized coupled climate experiment, abrupt4xCO2 (which features an abrupt quadrupling of CO_2 from preindustrial concentrations), seeking to verify whether the fast response of the circulation is detectable or if it is dominated by the response to the subsequent surface warming.

In summary, this study setup allows us to quantify and decompose the fast response of the tropical atmospheric circulation into the contributions of radiative cooling rate change and atmospheric stratification change. The comparison of the aquaplanet and Earth-like planet results is used to investigate whether the fast response of the circulation is dominated by the land–sea differential heating. The results presented here are based on an

ensemble of eight CMIP5 GCMs participating in both the aquaplanet and AMIP experiments. The analysis is concluded by comparing the change found in the atmosphere-only climate experiments with the change detected at different time extents in a coupled climate experiment. This way, we aim to identify the fast response signature in the total change of circulation.

This paper is structured as follows: Section 2 describes the data ensemble; section 3 gives a definition of the introduced circulation metric as well as the methodology to determine the contribution of the various parameters' change to the overall change in circulation intensity; results and discussion are contained in section 4; finally, section 5 draws conclusions and points out some considerations on further application of the findings.

2. Data

First, we use the monthly outputs of the CMIP5 aquaplanet idealized experiments (Taylor et al. 2012; Medeiros et al. 2015), namely, the aquaControl and the aqua4xCO2 experiments. The aquaplanet is an idealized Earth-size planet covered by water (no sea ice), with no axial tilting, and an atmosphere-only climate system with prescribed sea surface temperatures. The aqua4xCO2 experiment is set up based on aquaControl but with the CO_2 concentration quadrupled compared to the 1979–2008 historical mean (used in the aquaControl radiation scheme). Also, in this experiment, the surface temperature is prescribed to the aquaControl mean. Therefore, the climate system response in aqua4xCO2 represents the effect of the increase in CO_2 and is not subject to the change in surface processes resulting from increased surface temperature.

In the second part of the work, to account for the differential heating of land and sea surface, we investigate the monthly outputs of the atmosphere-only amip (from AMIP) and amip4xCO2 experiments (Taylor et al. 2012). For this case, an Earth-like planet is considered. In the amip experiment, the atmospheric composition follows the 1979–2008 mean historical values, and sea surface temperature and sea ice are prescribed to the 1979–2008 values. This experiment serves as a control for the amip4xCO2 experiment. As in the aqua4xCO2 experiment, in the amip4xCO2 experiment, the CO_2 concentration is quadrupled compared to its control experiment; the sea surface temperature is held fixed to the amip values, but the land is allowed to heat.

The length of the time series for both aquaplanet experiments is 5 years; for the amip experiments, it is 30 years. We apply the methodology described below on the time series mean of aquaControl, amip, and amip4xCO2 outputs. For the aqua4xCO2 experiment, we exclude the first year from the calculation as the climate system is strongly perturbed compared to the control run (under quadrupled CO_2), and these values are clear outliers compared to the 5-yr time series mean. The same perturbations do not affect the 30-yr mean in the amip experiments, therefore the first year is not excluded here. Throughout the study, we compare the mean control climate state (referred to onward as aquaControl/amip or control climate) with the quasi equilibrium reached by the climate system with quadrupled CO_2 concentration (referred to onward as aqua4xCO2/amip4xCO2 or forced climate).

In the last part of the investigation, we analyze the aqua4K and amip4K experiments (Taylor et al. 2012). These consider the same control climate as aqua4xCO2 and amip4xCO2, respectively, but the CO_2 concentration is maintained as in the control run, and only the sea surface temperature is uniformly increased by 4 K. To extend our analysis to coupled climate experiments, we use the CMIP5 abrupt4xCO2 experiment (Taylor et al. 2012). For this experiment, the CO_2 concentration is abruptly quadrupled compared to the preindustrial levels, and then it is kept constant, allowing the climate system to adjust and change toward a new state of equilibrium. The CMIP5 outputs for abrupt4xCO2 are typically limited to 140 years, even though only a quasi equilibrium is reached at this moment. As a control climate for this experiment, we use the piControl experiment results, featuring a climate system with atmospheric absorption species set to preindustrial levels (Taylor et al. 2012).

Within this study, we use the outputs of an ensemble of eight GCMs that were run for both aquaplanet and amip experiments as well as for the coupled ones: CCSM4 (Meehl et al. 2012), CNRM-CM5 (Voldoire et al. 2013), HadGEM2-A as the atmospheric component of HadGEM2-ES (Collins et al. 2011), IPSL-CM5A-LR (Dufresne et al. 2013), MIROC5 (Watanabe et al. 2010), MPI-ESM-LR (Stevens et al. 2013), MPI-ESM-MR (Giorgetta et al. 2013), and MRI-CGCM3 (Yukimoto et al. 2012). See Table S1 in the online supplemental material for more details on the GCMs.

3. Methods and tools

a. Methodology

We limit our analysis of the circulation change to the tropical subsidence regions. Following Davis and Birner (2013), the zero crossings between 20° and 40° latitude (in both hemispheres) of the vertically averaged zonal mean of the mass streamfunction are considered as the tropics' limits for any given time step (Fig. 1). This

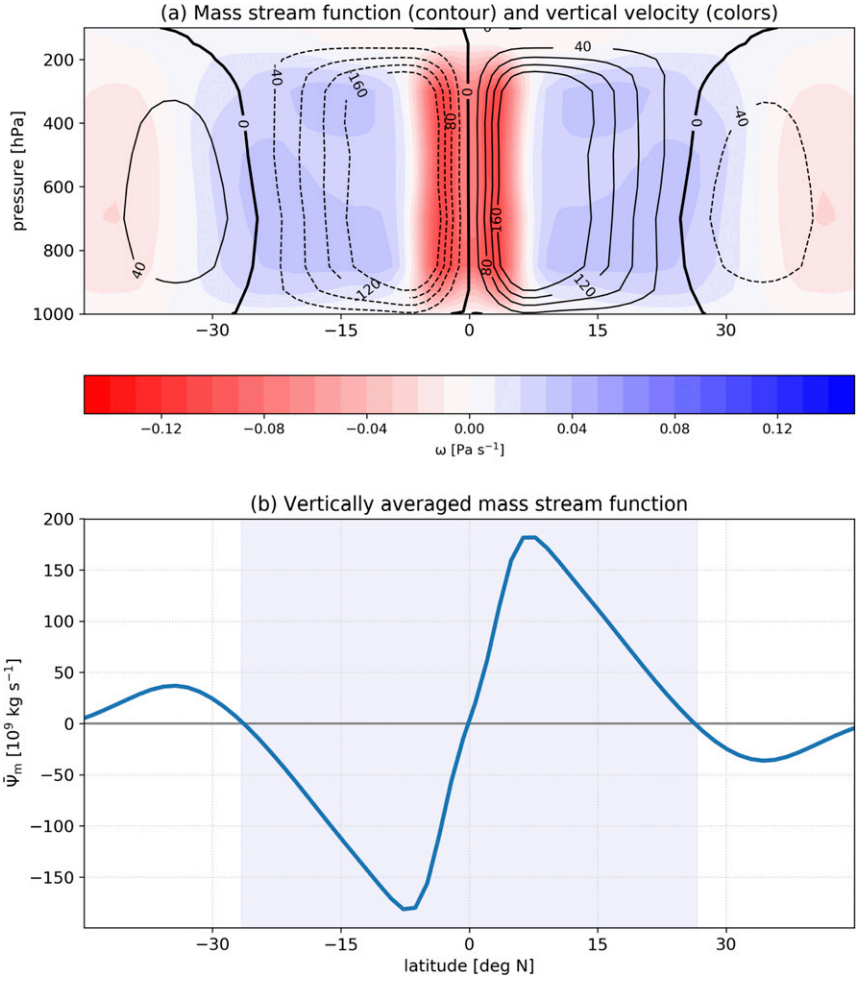

FIG. 1. (a) Zonal mean of the mass streamfunction (10^9 kg s^{-1}; black contours) and vertical velocity (color shading), averaged over the aquaControl output of MIROC5. (b) Vertically averaged zonal mean of the mass streamfunction for the same output.

allows the separation of the equatorward from the poleward air mass transport. An atmospheric column within the tropics is considered a subsidence column if the vertically averaged vertical pressure velocity $\overline{\omega}$ is positive.

In the limits of the detected tropical subsidence regions, we define the subsidence mass flow (SMF) as follows:

$$\mathrm{SMF} = \frac{1}{g} A{\downarrow}\omega, \tag{1}$$

where g is the gravitational acceleration, $A{\downarrow}$ is the subsidence area, and ω is the vertical velocity of each grid box. The SMF metric links to several other metrics, such as the metric used by Davis and Birner (2013) for the estimation of the tropical belt width or that used by Byrne and Schneider (2016a,b) for the width of the intertropical convergence zone (ITCZ), as these are all derived from a rearrangement of the tropical energy budget. The metrics from these previous studies, as well as our method, are therefore describing the subsidence and convective regions from the perspective of their dynamics and can be derived from GCM outputs less influenced by the model's parameterizations.

Figures 2(1)a and 2(1)b show the zonal mean of the subsidence mass flow averaged over the output of MIROC5 for the aquaControl and aqua4xCO2 experiments, respectively. It is noticeable that the spatial pattern of SMF is dominated by that of ω (Fig. 1a), as the gridbox area in the limits of the subsidence regions does not vary strongly enough to have an impact on the pattern of the subsidence flux. The patterns of SMF in the tropical subsidence regions are similar in all the investigated models (Fig. S1). However, they

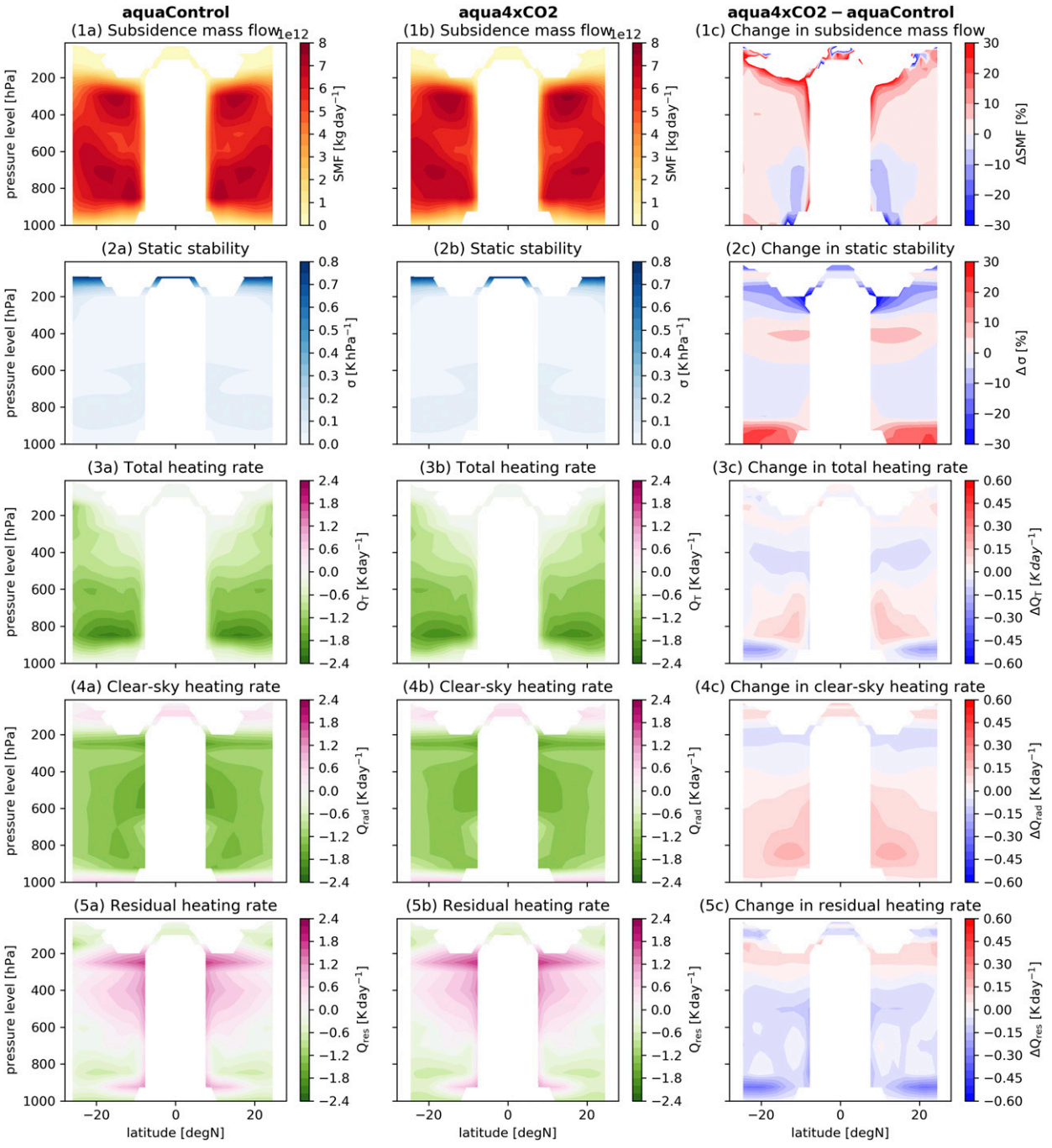

FIG. 2. (top row) Zonal mean of subsidence mass flow, averaged for MIROC5 over (a) the aquaControl and (b) the aqua4xCO2 experiment, as well as (c) the difference between the experiments. The remaining rows are as in the top row, but for static stability, total diabatic heating rate, radiative heating rate, and residual heating rate.

differ in the expansion of the subsidence regions, which relates to the presence of a double ITCZ in some models (CCSM4, CNRM-CM5, and IPSL-CM5A-LR; see Figs. S1, S2). Therefore, an ensemble mean exemplification of the zonal means shown in Fig. 2 would be misleading. (Note: The choice of the MIROC5 model for exemplification will be explained in the next subsection.)

In the tropical subsidence regions, the diabatic vertical motion ω balances the diabatic heating Q_T as horizontal temperature advection is almost negligible (Emanuel et al. 1994; Zelinka and Hartmann 2010;

Thompson et al. 2017). As this work is limited strictly to these regions, we diagnose vertical velocity from the total diabatic heating rate Q_T and static stability σ:

$$\omega = -\frac{Q_T}{\sigma}, \tag{2}$$

therefore Eq. (1) becomes

$$\mathrm{SMF} = -\frac{1}{g} A\downarrow \frac{Q_T}{\sigma}. \tag{3}$$

We decompose the tropical total heating rate Q_T into the purely radiative clear-sky heating rate Q_{rad} and a residual heating rate Q_{res}. The latter accounts for the cloud radiative effect, cloud microphysics, and the heating resulting from lateral eddy mixing (Phillips 1956) and is calculated for each profile as the difference between the diagnosed [from Eq. (2)] heating rate and the clear-sky heating rate, derived by using radiative transfer modeling (see section 3b),

$$Q_T = Q_{\mathrm{rad}} + Q_{\mathrm{res}}. \tag{4}$$

The definition of subsidence mass flow in Eqs. (1) and (3), and the consideration of Eq. (4) allow the decomposition of the change in subsidence mass flow as follows:

$$\frac{d\mathrm{SMF}}{\mathrm{SMF}} = \frac{dA\downarrow}{A\downarrow} - \frac{d\sigma}{\sigma} + \frac{dQ_T}{Q_T}, \tag{5}$$

and

$$\frac{d\mathrm{SMF}}{\mathrm{SMF}} = \frac{dA\downarrow}{A\downarrow} - \frac{d\sigma}{\sigma} + \frac{dQ_{\mathrm{rad}}}{Q_T} + \frac{dQ_{\mathrm{res}}}{Q_T}. \tag{6}$$

Therefore, we can investigate the relative change in SMF in comparison with the contribution of the relative change in the following parameters: subsidence area ($dA\downarrow/A\downarrow$), static stability ($-d\sigma/\sigma$), and heating rate (dQ_T/Q_T). The latter is also equivalent to the sum of changes in clear-sky heating rate Q_{rad} and residual heating rate Q_{res} relative to the total heating rate Q_T in the control setup ($dQ_T/Q_T = dQ_{\mathrm{rad}}/Q_T + dQ_{\mathrm{res}}/Q_T$).

This methodology will be applied to all the identified subsidence columns and only then will be averaged over the tropical subsidence regions. Therefore, it is probable that the averaging may introduce some small differences in the sums referred above [Eqs. (5) and (6), as well as in $dQ_T/Q_T = dQ_{\mathrm{rad}}/Q_T + dQ_{\mathrm{res}}/Q_T$].

b. PSrad

For the decomposition of total heating rate into the clear sky and residual components [Eq. (4)] we apply the radiative transfer package PSrad, introduced by Pincus and Stevens (2013) as post-scriptum of the radiation package of the Rapid Radiative Transfer Model for GCMs (RRTMG; Mlawer et al. 1997; Iacono et al. 2008), to calculate the clear-sky heating rate Q_{rad}. This package uses as input the vertical profiles for temperature, humidity, pressure, cloud properties, and absorption species' volume mixing ratios (CO_2, CH_4, N_2O, O_3).

The absorption species volume mixing ratios were not available for all the investigated GCMs. We therefore used mean profiles for the 1979–2008 period (from the output of the CMIP5 historical experiment; Taylor et al. 2012), averaged over MPI-ESM-LR, MRI-CGCM3, and four other GCMs that have available gas concentrations but are not investigated in this study (these GCMs were not run for the aquaplanet experiments): CanESM2 (Arora et al. 2011), CESM1(BGC) (Long et al. 2013), GFDL-ESM2G, and GFDL-ESM2M (Dunne et al. 2012). These profiles agree to a reasonable extent (Fig. S3). Nonetheless, we acknowledge that using an ensemble mean profile of absorption species instead of the GCM's native profile poses the risk that the PSrad calculations will not perfectly agree with the values we could obtain from the model output (see below for a comparison).

The GCM vertical profiles are limited in the stratosphere to 10 hPa. To account for this, we extend the remaining vertical range (10–0 hPa) with the tropical reference profiles from Anderson et al. (1986). These data provide stability to the PSrad run and ensure a realistic picture of heating rates above the tropopause without affecting the heating rate profile in the troposphere, which is our area of interest (see Fig. S4 for a comparison of PSrad run with and without using the reference profiles and note the unrealistic behavior of the heating rates toward the top of the atmosphere).

Besides the vertical data, PSrad uses surface temperature, surface pressure, surface albedo, and solar zenith angle as input. For surface albedo, we use the values of 0.07 for the ocean surface and 0.2 as a mean surface albedo for the tropical region. In the case of solar zenith angle, we have to account for the fact that the GCM output is a monthly mean output. Therefore, we follow Cronin (2014) and Wing et al. (2018) and use a fixed zenith angle of 42.05° and an adjusted solar constant of 456.07 W m^{-2} to ensure a tropical mean annual insolation.

To test the performance of PSrad on GCM outputs, we performed a comparison of these calculations of heating rates to the heating rates derived from the model output of atmospheric radiation fluxes. However, only one model from the eight investigated GCMs, MIROC5, had these data outputs available. The obtained values agree reasonably well: In the detected

subsidence regions, the differences between the calculated profiles are around $\pm 0.5\,\mathrm{K\,day^{-1}}$ (Fig. S4) and relate to the usage of ensemble mean profiles for absorption species, the nonlinear calculations in PSrad, and spatial averaging. In the convective regions and in the stratosphere, the differences are considerably larger, but as these are not our regions of interest, we did not pursue an investigation in this direction. To ensure consistency, we use MIROC5 for exemplification throughout the study, without considering it special compared to the other members of the ensemble.

4. Results and discussion

This section includes the discussion of the detected circulation change, as well as the decomposition of this change into the contributions of radiative heating rate, stratification, and subsidence area change for the aquaplanet experiments (section 4a) and the amip experiments (section 4b). The comparison of these results with those found in the atmosphere-only experiments with 4-K increase in sea surface temperature and in the coupled abrupt4xCO2 experiment are presented in section 4c.

a. Aquaplanet experiments

Because of the lack of landmass and seasons, the aquaplanet climate system is fairly symmetric meridionally and fairly uniform zonally. This enables the investigation of various variables just by looking at their zonal means. We use the MIROC5 results to illustrate the zonal means for the subsidence mass flow, static stability σ, heating rates (total Q_T, clear sky Q_{rad}, and residual Q_{res}), and their difference between aqua-Control and aqua4xCO2 (Fig. 2). Note that the difference for the subsidence mass flow and static stability is shown in percentage, while for the heating rates it is in kelvins per day. The latter have both negative and positive values, confusing the assessment of the change. The results indicate that in an aquaplanet setup, the changes due to CO_2 quadrupling occur with respect to the magnitude not the latitudinal pattern of the various variables. In the case of MIROC5, the detected changes are quite symmetrical with respect to the equator. This is not the case for all models (Fig. S1), where the asymmetry is quite evident. Such a result may relate to the model's representation of atmospheric waves and the heat/moisture transport at the edges of the tropics, as well as to the insufficient length of the run, which does not ensure an equilibrium state for the climate system with quadrupled CO_2.

The subsidence mass flow, and therefore the circulation, is in general weakening (Fig. 2, top row; Fig. S1), which is in agreement with previous studies (Held and Soden 2006; Vecchi and Soden 2007; Bony et al. 2013; He and Soden 2015). The region where the values increase in most GCMs (Fig. S1) is in the vicinity of the ITCZ, suggesting that this convective region narrows. This is consistent with previous studies reporting this narrowing in Earth-like planet experiments (Lau and Kim 2015; Byrne and Schneider 2016b). A small change is seen in the static stability in the midtroposphere (Fig. 2, second row), but the upper troposphere and the surface boundary layer show a clear increase in stability. The detected response in the upper troposphere may be related to the increase in high clouds and the rise of the level of maximal meridional mass outflow in the upper troposphere, which enhance moisture divergence at these levels and promote a stability increase (Zelinka and Hartmann 2010; Lau and Kim 2015), but a further investigation of cloud and moisture fields is beyond the scope of this paper. Such a considerable increase in static stability in the surface boundary layer is only found for MIROC5 (not shown), suggesting that the parameterizations of the surface processes are the most probable cause. The positive change in total heating rate, concentrated around 850 hPa (Fig. 2, third row), suggests that the atmosphere cools less in the forced climate. This response is dominated by the change in Q_{rad} (Fig. 2, fourth row), while the change in Q_{res} (Fig. 2, bottom row) appears to dominate the response of Q_T in the upper troposphere, as well as close to the ITCZ. Such a distribution of change links again to the adjustment of (high) clouds to quadrupled CO_2 and suggests a narrowing of the ITCZ and a drying of the atmosphere by entrainment in the regions close to the edges of the ITCZ. Note that the parameters' values in the layer above the surface and in the stratosphere are either impossible to compute for all GCMs (these regions have little to no subsidence) or are too scattered to present a clear picture. Therefore, for further analysis, we consider only the results for the troposphere at pressures below 925 hPa.

Figure 3 shows the ensemble mean tropical subsidence profiles for SMF, σ, $A\downarrow$, Q_T, Q_{rad}, and Q_{res} for the control climate and the forced climate. The difference between the profiles confirms once more that the circulation weakens, most prominently in the lower part of the troposphere. As the surface is not allowed to heat, which would impact the lapse rate, the direct effect of CO_2 increase on the mean static stability is almost undetectable. This is not the case for the subsidence area and heating rates. The subsidence area increases throughout the height of the troposphere. In the case of Q_T, the change is driven by the change in Q_{rad}, which shows a weaker atmospheric cooling in the lower and midtroposphere.

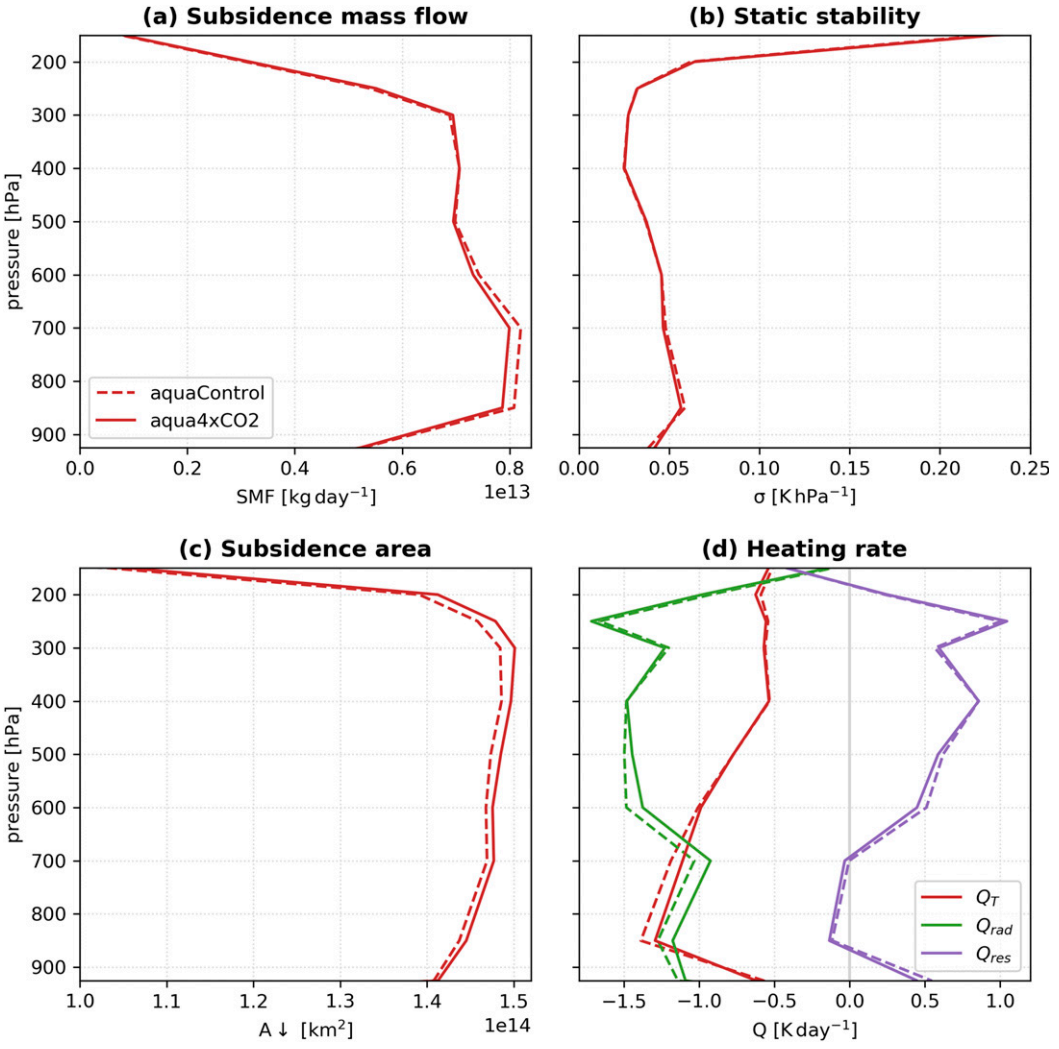

FIG. 3. The aquaControl (dashed lines) and aqua4xCO2 (solid lines) ensemble mean profiles of (a) subsidence mass flow, (b) static stability, (c) tropical subsidence area, and (d) total, clear sky, and residual heating rates (the profiles are averaged over the tropical subsidence areas).

Taking into account the spatial patterns observed in Fig. 2, we could assume that these patterns in the subsidence region may also be impacted by the CO_2 forcing. However, by analyzing, for each GCM, the ratio between the standard deviation and the mean of all the tropical subsidence vertical profiles in the control and the forced climate, respectively (not shown), we find that this ratio does not show any considerable change under forcing. Therefore, the increased CO_2 has an effect on the mean climate state without changing the spatial pattern in the subsidence regions. Moreover, in the tropical subsidence regions, regardless of the forcing, the vertical profiles of the parameters vary within the range of 2.5 standard deviations around the mean profile, and the profiles within the 5th–95th percentiles are within 1.8 standard deviations from the mean. These findings support our choice to use the mean profile as a representative of the tropical subsidence region.

After investigating the response of each variable to CO_2 forcing, we now look at the contribution of the respective change to the general change in tropical overturning circulation (Fig. 4). According to Eqs. (5) and (6), a relative increase in subsidence area and in heating rate will force an increase in circulation intensity, while an increase in static stability will dampen the circulation. As mentioned above, the circulation weakens considerably in the lower and midtroposphere. We find that this weakening is of 3%–5% in the ensemble mean (Fig. 4a; red line), and the ensemble spread of the maximum decrease in circulation strength is 1%–8%

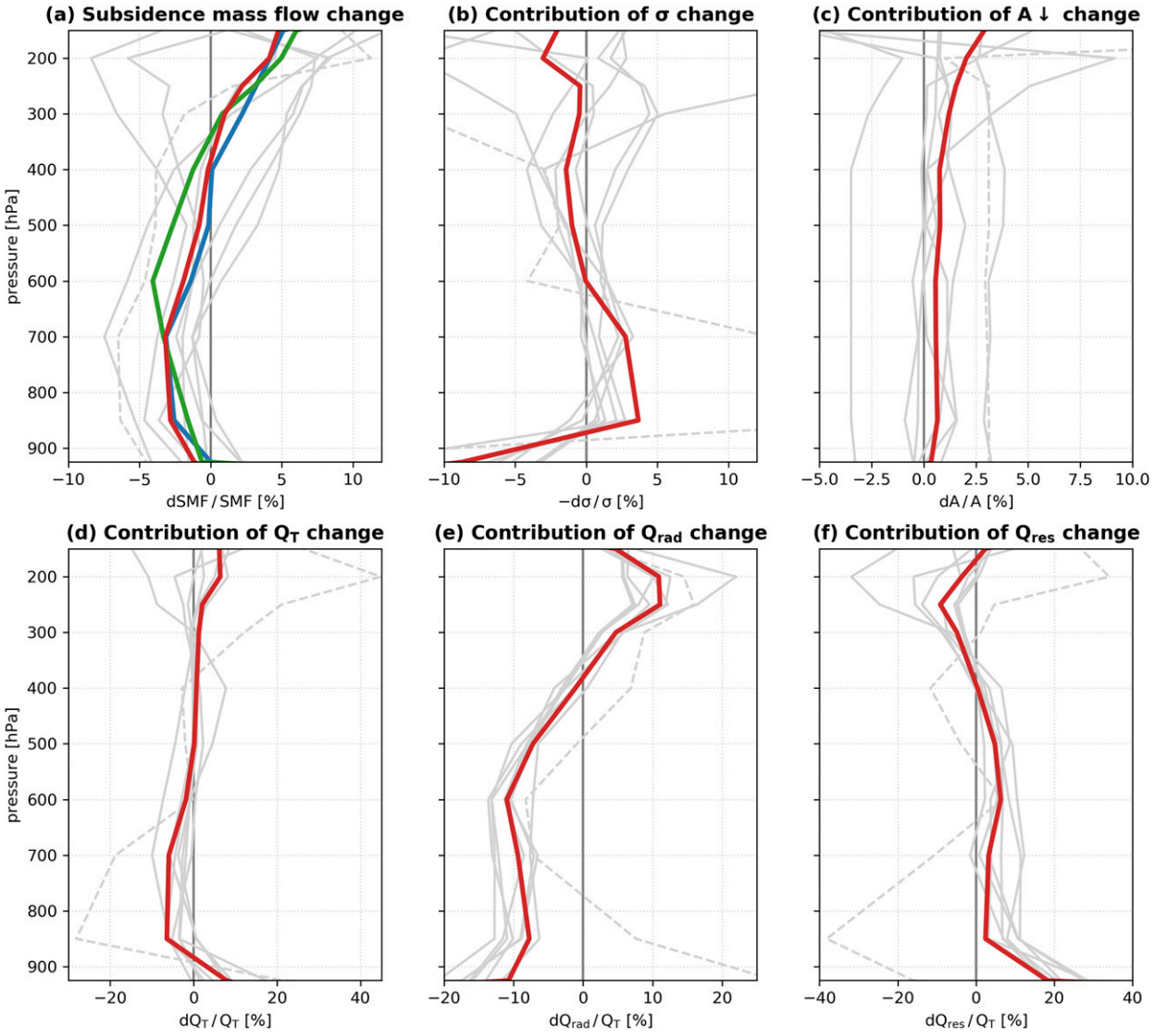

FIG. 4. (a) Relative change of subsidence mass flow in the aquaplanet experiments. The solid lines present a comparison of this change calculated following Eqs. (1) in red, (5) in blue, and (6) in green. The contribution to the change in SMF of (b) static stability change, (c) subsidence area change, and (d) total, (e) clear sky, and (f) residual heating rate change. The gray lines represent the corresponding results for every ensemble member [in (a) they show the change in SMF according to Eq. (1)]. Note: The dashed gray line corresponds to HadGEM2-A.

(Fig. 4a; gray lines). It needs to be mentioned that the slowdown of the circulation in the 700–800-hPa layer appears to be a robust feature of this ensemble, but above this layer, there are some models that suggest a strengthening of the circulation. This model spread in the circulation change resembles the spread in the contributions of the static stability and subsidence area changes (Figs. 4b,c). The static stability and subsidence area response to CO_2 forcing bring, on the mean, around 4% and 1% enhancement to the circulation, respectively. However, especially in the upper troposphere, the model spread suggests that a positive contribution to the circulation change may not be a robust result and that it is highly dependent on the GCM. This could be reinvestigated once there is a larger ensemble of GCMs available. On the mean, we find that the positive contributions of σ and $A\downarrow$ to the change in circulation are counteracted by the CO_2 effect on the total heating rate (Figs. 4d–f): Q_T decreases by 7%–8% and causes a general weakening of the circulation. The change in total heating rate is dominated by the change in clear-sky heating rate, which is reduced by around 10%. However, above 400 hPa, the total and radiative heating rates become slightly more negative (the atmosphere cools more). These findings, together with the ensemble spread found in Figs. 4b and 4c,

explain the slight increase in SMF in the upper troposphere, suggesting stronger subsidence. This result also goes in line with the narrowing of the ITCZ, which intensifies the convection and the divergent mass flow at the tropopause height, with subsequent subsidence increase in the tropical upper troposphere. We note that Figs. 4b–4f show a clear outlier: HadGEM2-A. This may represent an effect of the model's inability to accurately represent tropical low-cloud fields and precipitation processes (Haywood et al. 2016). However, the profile of SMF change for this model does not stand out notably within the ensemble spread (Fig. 4a), which seems to be related to the fact that the effects of static stability change and diabatic heating rate change balance each other in the lower troposphere.

Considering the above, we find that the fast response of the tropical overturning circulation to CO_2 quadrupling in an aquaplanet setup exhibits a weakening of around 4%, similar to the one found by He and Soden (2015), but based on a method using the convective mass flux to quantify the circulation intensity. This weakening can be decomposed into a sum of contributions from static stability, subsidence area, and heating rate. Figure 4a shows that the calculated relative change in subsidence mass flow can be reasonably well approximated by the sums of contributions, as presented in Eqs. (5) and (6). However, the sum from Eq. (6) is deviating stronger from the calculated change, and this is most probably related to the calculation of Q_{rad} with PSrad, as we use the same mean profiles of absorption species for all GCMs. Based on this decomposition, we find that the driver of the change in circulation is the radiative effect of CO_2 on the clear-sky heating rate, reconfirming previous studies (Bony et al. 2013; He and Soden 2015). The results from the ensemble GCMs still vary considerably because of the model configuration and initialization, visible even in the tropical mean surface temperature, which has a spread of 293.8–296.5 K in the control climate (not shown). But the resulting ensemble variance in the change of the investigated variables supports the robustness of the circulation weakening.

b. *AMIP experiments*

In this section, we perform a similar analysis as above but for Earth-like, atmosphere-only climate systems, described through the amip and amip4xCO2 idealized experiments. This time, we look only into the mean profiles, averaged over the subsidence areas, without investigating the zonal means, as we did above with Fig. 2. The decision relates to the much less spatially uniform (and therefore less zonally representative) subsidence regions on a planet with landmass and orography (see Fig. S5 for an exemplification based on MIROC5). Though not addressed in this paper, a thorough investigation of the changes in the distinct large subsidence regions over the Pacific and Atlantic Oceans would lead to a better understanding of the changes in the dynamics of the subsidence and the subsequent impact at a regional scale.

In comparison with the aquaplanet experiments, in the amip experiments we find that, on the mean, the circulation weakens throughout the troposphere in response to CO_2 increase, not only in its lower part (Figs. 5, S6). This more uniform tendency is driven by the different change pattern between the subsidence areas over land and over ocean. The change over the ocean is similar to the aquaplanet results: Most of the change is projected for the lower troposphere. Over land, however, we detect a substantial weakening in the upper troposphere as well. This finding is related to the increasing land surface temperatures and their effect on the air column above. Another difference between the aquaplanet and amip experiments is in the circulation intensity itself: The aquaplanet has a much more vigorous circulation in the tropics. The setup of the experiments easily explains this result, as the aquaplanet has no axial tilting and therefore the tropics receive the same amount of solar energy year-round compared to the amip realistic planet system. This aspect can also explain the static stability profiles' difference between amip and aqua experiments. Judging by the height of the sudden increase in static stability, the tropopause is, on the mean, situated higher in the aquaplanet system than in the amip system (Figs. 5, S6). However, this does not change the response of σ to CO_2 quadrupling, as its profile barely changes. The differential heating of land and ocean in the amip experiments leads to opposing tendencies in the subsidence area under increased CO_2 forcing: It shrinks over land and expands over ocean (Figs. 5, S6), as was shown previously by Bony et al. (2013). Nonetheless, the total tropical subsidence area change is driven by the change over ocean, as here the area is around 3 times as big as the area over land. The heating rates have similar values in the aqua and amip experiments, as well as the same tendencies: We find again a less-cooling atmosphere in the forced climate (Figs. 5, S6). There is, however, a clear difference between experiments for the residual heating rates, which are larger in the amip experiment, especially in the lower troposphere. This difference between the aqua and amip experiments, as well as the larger difference within the amip experiments, may be related to a different cloud regime and a more irregular flow on a planet with land surfaces and to the response of the extratropical systems to CO_2 forcing. Such a response is the equatorward shift of the storm tracks and increased lateral eddy mixing (Butler et al. 2010). A follow-up on

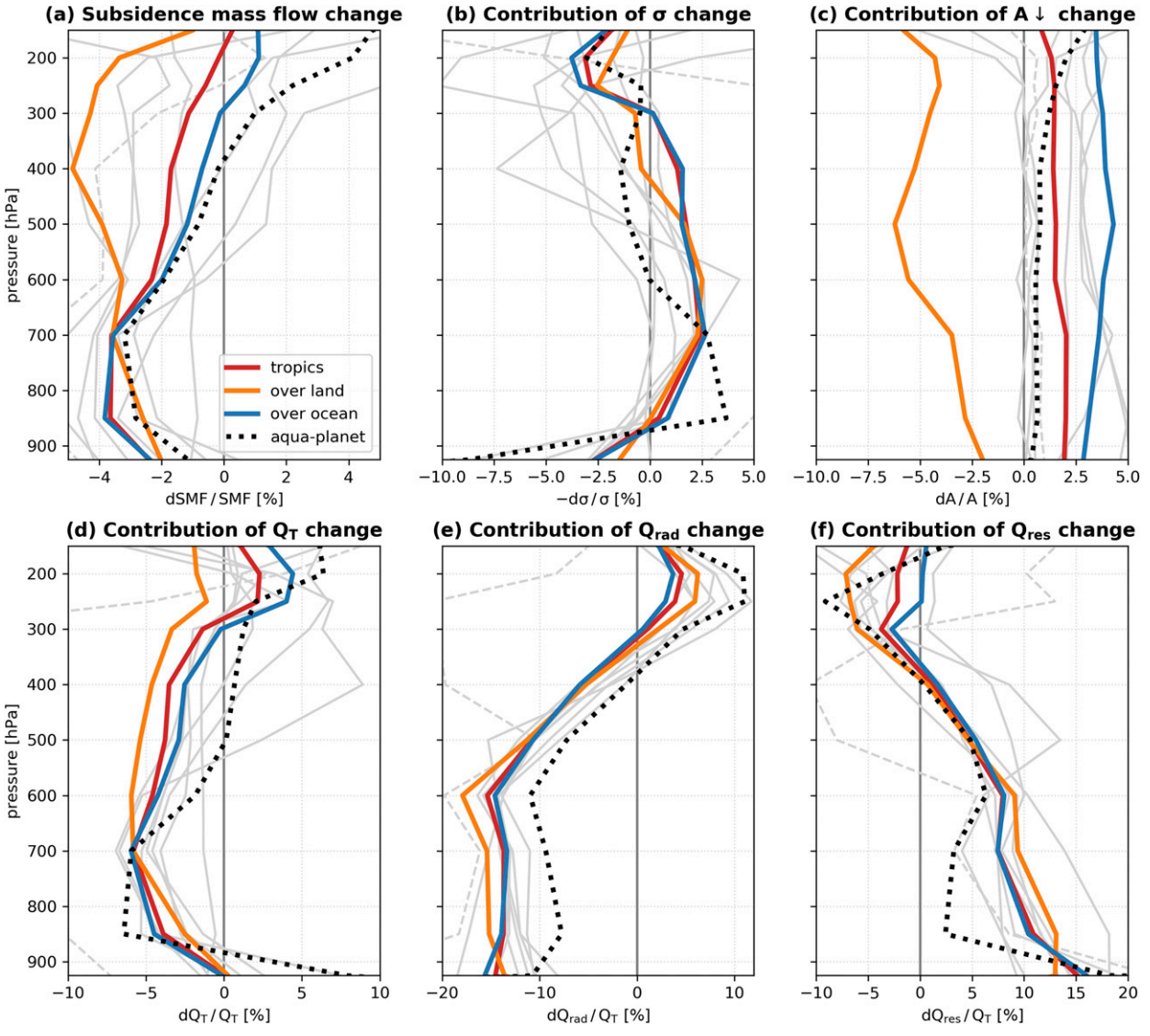

FIG. 5. (a) Relative change of subsidence mass flow in the amip and amip4xCO2 experiments. The contribution to the change in SMF of (b) static stability change, (c) subsidence area change, and (d) total, (e) clear sky, and (f) residual heating rate change. The respective results are presented for the entire tropical subsidence area (red lines), as well as over land (orange lines) and over ocean (blue lines). The results from the aquaplanet experiments are presented in dotted black lines for comparison. The gray lines represent the corresponding results for every ensemble member [in (a) they show the change in SMF according to Eq. (1)]. Note: The dashed gray line corresponds to HadGEM2-A.

this feature is possible with an analysis of the change in cloud and moisture dynamics, but at the moment is beyond the aim of this study.

As mentioned earlier, there is a much more vertically uniform change in circulation (subsidence mass flow) in the amip experiments in comparison to the aquaplanet experiments. As can be seen from Fig. 5, overall in the tropics, this change amounts to 3%–4% in the lower troposphere and is dominated by the change over ocean. Toward the tropopause, the general change decreases to 0%; in comparison, in the aquaplanet experiments, we find an increase of around 3% near the tropopause. Here, the pattern is largely impacted by the change over land, where the circulation decreases uniformly throughout the troposphere by around 4%. Such a difference between the lower and upper troposphere in comparison to the aquaplanet experiments is noticed in the other variables too. However, this does not impact our findings related to the main contributor to the circulation weakening: In the amip experiments, we find that it is again the decrease of the radiative heating rate that dominates the circulation variation.

Although the amip experiments' setup introduces additional sources for the potential tropical circulation change, we find that, regardless of the presence of land–sea contrast, the circulation weakens. The main driver of this change in the amip case is also the direct effect of CO_2 increase on the radiative heating rate. However, the differential heating of land and ocean impacts the vertical distribution of this weakening by not limiting it to the lower troposphere.

c. *The fast response signature in a coupled climate system*

A comparison of the fast response of the circulation with its response to the surface warming induced by the CO_2 increase, in atmosphere-only and coupled experiments, can further the understanding of the time and space scales of the atmospheric dynamics response to anthropogenic forcing without limiting the contributions to the atmospheric processes only.

We will refer henceforth to the combined actions of the greenhouse effect amplification and the subsequent climate system feedbacks as the slow response of the circulation to increased CO_2 forcing. The advantage of the CMIP5 tiered experiments is that we can separately investigate the effects of CO_2 and the subsequent (slower) increase in surface temperature by analyzing the results from the aqua4xCO2/amip4xCO2 and aqua4K/amip4K experiments. This comparative investigation will further our understanding of the changes detected in the coupled abrupt4xCO2 experiment, in which the impact of the factors combine.

We continue the research approach from the previous subsections by assessing the change in circulation induced by a uniform increase in sea surface temperature by 4 K. We find that the effect of this increase is a stronger slowdown (of up to 12% in the upper troposphere) of the tropical circulation compared to the effect of CO_2 (Fig. 6a). The vertical pattern of change is again different between the aqua- and the Earth-like planets. Under the presence of land, the circulation changes nonuniformly on the vertical: In this case, the intensity decreases considerably in the upper troposphere, while in the lower troposphere, it is close to the change induced by the quadrupling of CO_2.

The impact of the surface temperature rise on the static stability, subsidence area, and diabatic heating rate determines again clearly the vertical pattern of change in circulation (Figs. 6b–d). The static stability increases notably compared to its response to CO_2 forcing. But the land–sea contrast appears to have an effect on the change in the lower troposphere, where the increase in static stability is around half as strong as in the upper troposphere (in the aquaplanet experiment there is also less increase in the lower troposphere, but the difference to the upper troposphere is smaller). Compared to aqua4xCO2/amip4xCO2, in the aqua4K/amip4K experiments, the subsidence area increases considerably: The difference to the control is 10–12 times larger in the aquaplanet experiments and 3–4 times larger in the amip experiments. Whereas the total diabatic heating rate mostly increases as a response to CO_2 quadrupling, it becomes more negative when the surface heats: The atmosphere cools more strongly by up to 0.2 K day^{-1} in the upper troposphere. This change is dominated largely by the response of the radiative heating rate to forcing (Figs. 6d,e).

We find that the circulation weakens by 0%–5% in the lower troposphere and that this response is dominated by the weakening over the ocean (Fig. 6a). In the upper troposphere, the weakening is more intense: up to 12%. Here, compared to the effect of CO_2 increase, the change in radiative heating rate leads mostly to a strengthening of the circulation (Fig. 6a), except in the midtroposphere. We can speculate that here the atmosphere cools less radiatively, but this effect is counteracted diabatically by the advection of dry air, as suggested by Lu et al. (2008). As a result, the total heating rate change as a result of surface warming has a positive effect on the circulation (Fig. 6d). The same goes for the subsidence area change that increases by around 6% and is dominated by the considerable increase over land (Fig. 6c). However, these positive contributions to the circulation response are not sufficient to dominate the negative contribution resulting from the increase in static stability. The latter increases by around 12% in the lower troposphere and by up to 60%–70% in the upper troposphere (Fig. 6b), driving the overall vertical pattern of the circulation slowdown.

As we see above, there are two main mechanisms driving the circulation weakening in a realistic climate system: the atmosphere cooling less as a result of the CO_2 forcing increase and the enhanced static stability as a result of the rise of surface temperature. These effects are related but occur in different time frames and in different layers of the troposphere: In the lower and midtroposphere, both mechanisms mostly contribute to the circulation slowdown, while in the upper troposphere this slowdown is evidently driven by the increase in static stability.

Considering a coupled climate system in which the concentration of CO_2 is abruptly quadrupled and then kept at the same level (the abrupt4xCO2 CMIP5 experiment), we find that the surface temperature starts increasing immediately, considering climate time scales, by up to 1 K in the first year (not shown). However, because of the slow rate of CO_2 exchange between the

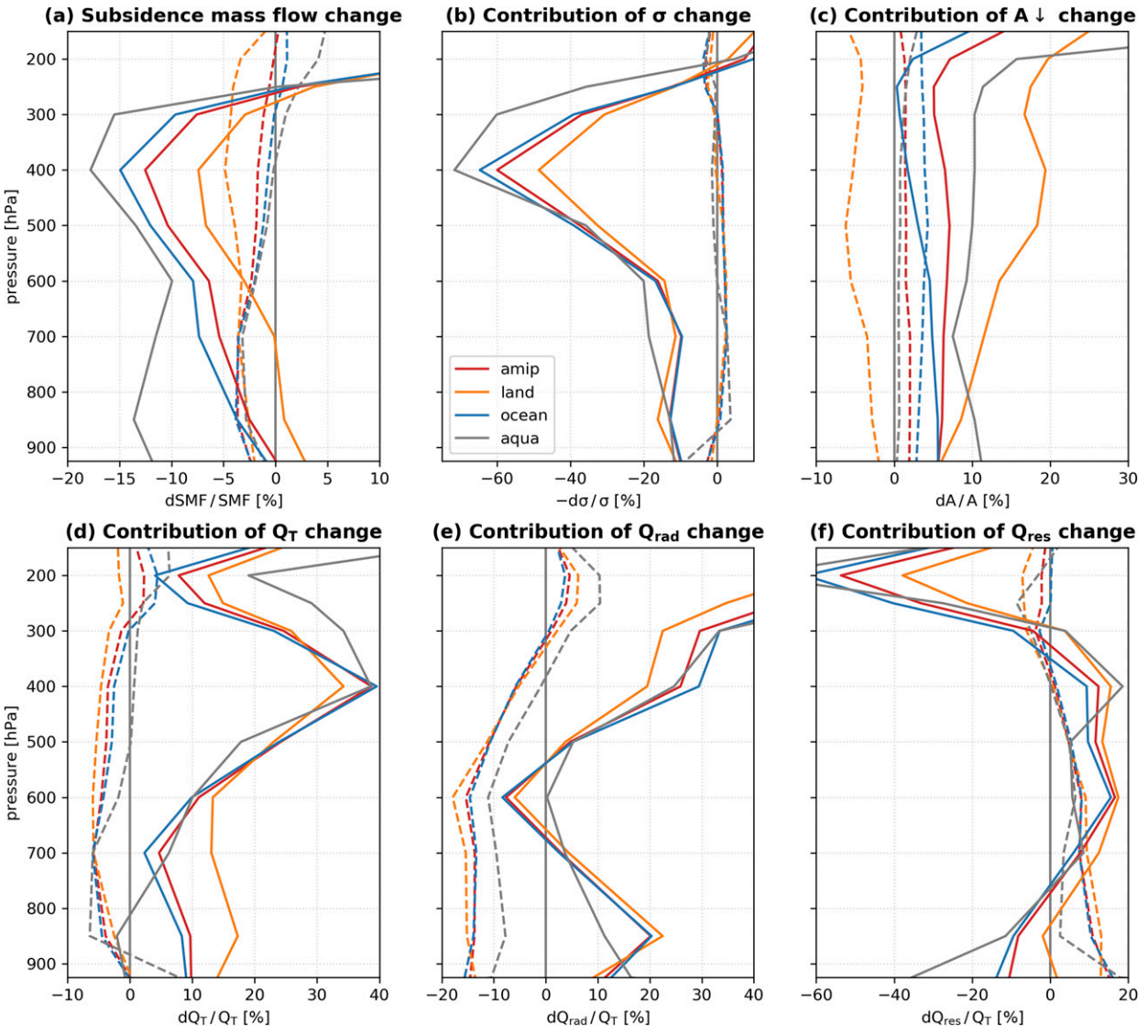

FIG. 6. Ensemble mean tropical profiles of relative change in (a) subsidence mass flow, (b) static stability, (c) tropical subsidence area, and (d) total, (e) clear sky, and (f) residual heating rates. The gray lines refer to the aquaplanet experiments, the red lines to the mean tropical profile in the amip experiments, the orange lines to the mean profile over land, and the blue lines to the mean profile over ocean. The dashed lines present the respective profile in the experiment with quadrupling of CO_2 and the solid lines in the experiment with 4-K increase in sea surface temperature.

surface waters and the deep ocean, it takes more than 50–200 years for the system to reach a quasi equilibrium. In view of these distinct time frames, a brief investigation of the response of the circulation in a coupled climate system will be carried out here by comparing the means over the first year after CO_2 quadrupling, as an immediate response to the forcing, with the means over the last 30 years of the experiment run (years 110–140), as a quasi-equilibrium climate state.

The changes in the circulation intensity and the contributors to the change are shown in Fig. 7 for the first year and for years 110–140 in abrupt4xCO2 compared to the responses detected in the amip4xCO2 and amip4K. Although in the first year after the CO_2 quadrupling the circulation does not exhibit substantial change, the resulting slowdown of up to 18% in intensity (in the upper troposphere) at the moment of quasi equilibrium indicates the considerable role the anthropogenic CO_2 forcing has on the atmospheric dynamics in the tropics. Note that the impact of CO_2 increase is still detectable in the first year of the coupled experiment, as the radiative heating rate vertical profile of change is similar to the amip4xCO2 profile. Notably, the mean profile of change for the last 30 years of the experiment indicates to the

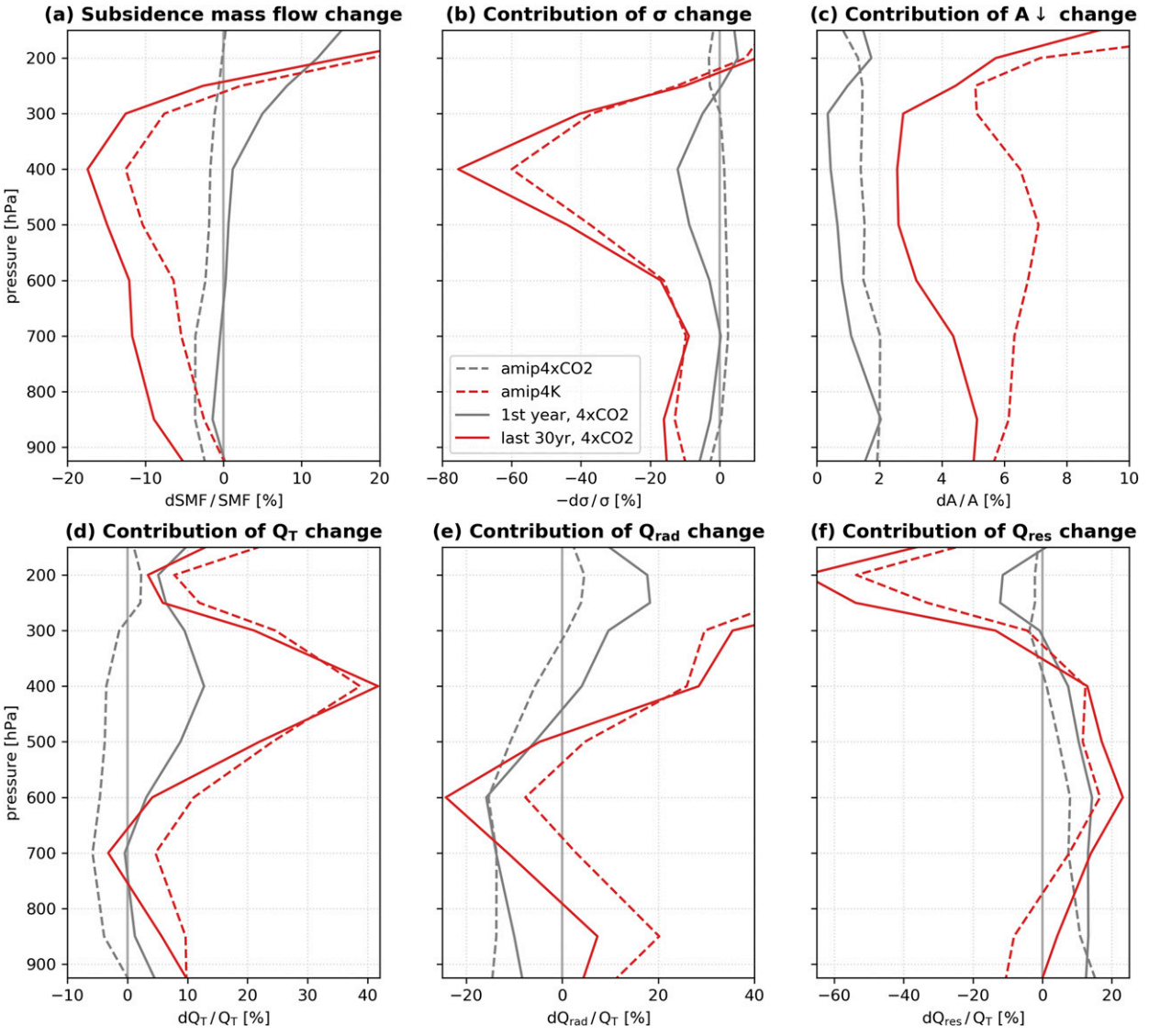

FIG. 7. Ensemble mean tropical profiles of relative change in (a) subsidence mass flow, (b) static stability, (c) tropical subsidence area, and (d) total, (e) clear sky, and (f) residual heating rates. The dashed lines refer to the amip experiments (gray lines for amip4xCO2 and red lines for amip4K), the solid lines to the abrupt4xCO2 coupled experiment (gray lines for the first-year mean in abrupt4xCO2 and red lines for the last 30-yr mean in abrupt4xCO2).

effect of the increased surface temperature on the heating rate (Fig. 7e). In the case of the static stability change, the effect of the increase in temperature is observed already in the first year (Fig. 7b). Therefore, the fast response of the circulation to CO_2 can still be detected at time scales smaller than one year, consistent with the findings of Bony et al. (2013). However, it is also noticeable that the circulation barely changes in the first year. The fact that in the first year the positive contribution of residual heating rate change is comparable to the sum of the negative contributions of the change in static stability and radiative heating rate (Fig. 7) suggests that the adjustment of the cloud systems and air masses exchange to the increased forcing occurs at this time scale and has a considerable impact on the circulation.

In Fig. 8, we present the impact of the two mechanisms of circulation change for every month in the first 10 years of the abrupt4xCO2 run (for consistency reasons again presented on the example of MIROC5). A seasonal cycle becomes evident in the evolution of the profiles: In boreal winter, the tropical midtroposphere cools less, while the upper troposphere cools considerably more in boreal summer, and these changes amplify with time. This behavior seems to be related to the change in Q_{rad} in the upper troposphere: The change over land and ocean diverge more strongly from the mean profile in

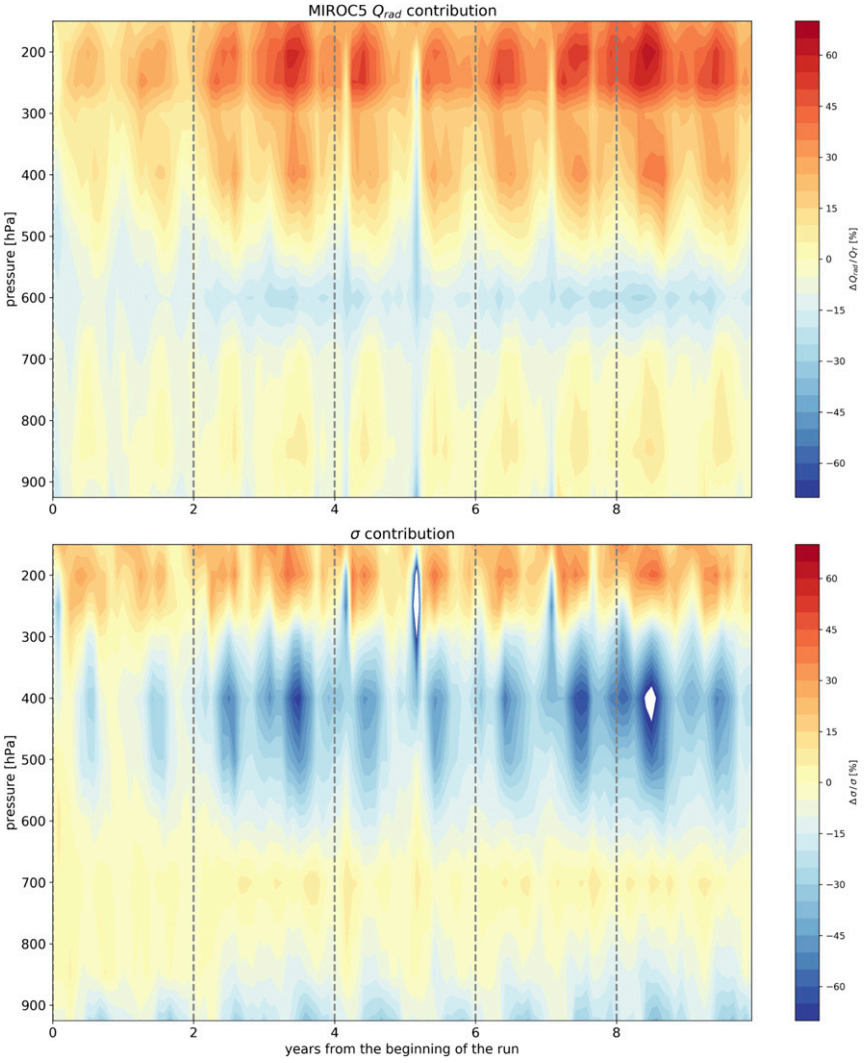

FIG. 8. Time–space representation of the contribution of (top) clear-sky heating rate Q_{rad} change and (bottom) static stability σ change to the tropical circulation change, shown for every time step (monthly means) in the first 10 years after the beginning of the abrupt4xCO2 run for MIROC5.

this layer. Therefore, the seasonal change of the land-to-ocean ratio in the tropics would impact the time evolution of the Q_{rad} contribution to circulation change. The same appears to hold for the contribution of σ change, which has a larger difference between the mean, overland, and overocean profiles in the upper troposphere.

We concluded above that the fast response of the circulation to CO_2 is still detectable at time scales smaller than one year. We also notice this in Fig. 8 in the first months, when the static stability decreases slightly (and has a positive contribution), while the atmosphere is cooling less up to 400 hPa. In other models, these first 3–5 months are even more evident (see Fig. S7 for MPI-ESM-LR), therefore an investigation of a larger ensemble would be an obvious outlook for this study. After these first months, the enhancement of the static stability in the upper troposphere becomes more evident, which also drives the general vertical pattern of change in circulation intensity.

Concluding, we found that the likely tropical circulation weakening as a result of increased CO_2 forcing is driven by different mechanisms depending on the investigated time and space frame. In the first months after a hypothetical sudden increase in CO_2 concentration, the circulation will respond first to the radiative effect of CO_2, that is, the decreased atmospheric cooling rate. But the rapid increase in surface temperature would enhance the static stability, especially in the upper troposphere, quickly enough for this effect to be

detectable (and to overtake the fast response) one year after the concentration increase.

5. Conclusions

Here, we investigated the fast response of the tropical overturning circulation to CO_2 forcing. The analysis was performed on an ensemble of eight GCMs for the CMIP5 aquaplanet and amip experiments with CO_2 quadrupling from control levels but with fixed sea surface temperature. We define a new metric for the circulation, the subsidence mass flow, which characterizes the subsidence strength in the tropics. In addition to the assessment of the change, this metric allows the quantification of the contribution of various processes to the total circulation change. By limiting our analysis to the subsidence regions, we reduce the impact of uncertainties arising from the GCM precipitation and convection parameterizations on our results.

We have confirmed that the tropical circulation weakens with rising CO_2 concentration, even when surface temperature is held fixed, as has been argued by Bony et al. (2013). In our metric, the weakening is 3%–4% for a quadrupling of the CO_2 concentration, similar to the results of He and Soden (2015). The driver of this change is the CO_2 radiative effect on the atmospheric heating rate: The atmosphere cools less (by up to 15%) with larger CO_2 content, reducing the radiatively driven subsidence. This change in radiative heating rate dominates the opposing positive contributions of static stability change (up to 2%–4%), subsidence area expansion (up to 1%–2%), and residual heating rate (up to 5%–9%). This result is similar in both the aquaplanet and the amip experiments: The direct radiative effect of CO_2 dominates the circulation change also for the planets with a land surface and overshadows the land–sea contrast changes. Nonetheless, the differential land–ocean heating in the amip experiments impacts the vertical pattern of circulation change. Here, we find that the weakening of the tropical circulation is not limited to the lower troposphere but extends (gradually becoming smaller) toward the tropopause. Such a pattern is driven by the surface heating over land and the subsequent change in radiative fluxes throughout the atmospheric column. We also notice that the results obtained in the amip experiments over ocean are not entirely similar to the aquaplanet results. This may relate to the regional land–sea boundary interactions (Kamae et al. 2014) and a stronger dynamical variability in the Earth-like climate system. The variation patterns found here are similar in most of the ensemble members, which indicates a likely robustness of our findings, even though the study was limited to the eight CMIP5 models that performed the aquaplanet experiments.

By comparing these results with those from atmosphere-only climate experiments with only an increase in surface temperature, we found a distinct mechanism leading to the slowdown of the circulation as well. In this case, it is the increase in static stability that dominates the response of the circulation. By furthering the analysis to an idealized coupled experiment, we note that at time scales smaller than one year, the role of the first mechanism of circulation change (the decreased atmospheric cooling) is still detectable but is quickly overtaken by the second mechanism resulting from the surface temperature rise in response to the greenhouse effect. Supplementary to this, we note that in a coupled climate system, the tropical atmospheric circulation changes most prominently in the upper troposphere. This may explain previous results from Plesca et al. (2018) on the robustness of the weakening of the Walker circulation: Such a response to CO_2 forcing is a more robust feature of climate change if the metric used for quantifying the circulation intensity is derived from upper-tropospheric variable fields, which are less sensitive to surface processes.

In outlook, our analysis may be extended to investigate the relative contributions of heating rate change and stratification on the circulation change in a larger ensemble of coupled climate simulations. This would further the understanding of the fast response of the atmospheric dynamics to anthropogenic CO_2 forcing without limiting the contributions to the atmospheric processes only. In addition, the metric proposed here focuses on the subsidence regions. These regions benefit from less contamination of the radiative signal because of the reduced amount of clouds and increased atmospheric stability. They are easily observable with spaceborne instruments and offer a less uncertain view on the radiative fluxes than the cloudy regions (Pincus et al. 2015). Our SMF metric may therefore prove efficient in tracking the circulation changes in the present climate by analyzing satellite data records.

Acknowledgments. We acknowledge and are grateful for the contribution to this paper of the late Dr. Verena Grützun. Elina Plesca was supported through the Cluster of Excellence CliSAP (EXC177), Universität Hamburg, funded through the German Science Foundation (DFG). Stefan A. Buehler was partially supported by DFG Research Group 1740 (Contract BU2253/1-2), by BMBF project HD(CP)^2 (Contracts O1LK1502B and O1LK1505D), and by the DFG HALO research program (Contract BU2253/3-1). We thank the World Climate Research Programme's Working Group on Coupled Modelling, responsible for CMIP5, and the institutions responsible for the models used here. The CMIP5 data were accessed through the German Climate Computing Centre (DKRZ)

ESGF-CoG node. We also thank Bjorn Stevens and Chris Bretherton for the constructive discussions about the findings of this study.

REFERENCES

Anderson, G. P., S. A. Clough, F. X. Kneizys, J. H. Chetwynd, and E. P. Shettle, 1986: AFGL atmospheric constituent profiles (0-120 km). Air Force Geophysics Lab. Tech. Rep. AFGL-TR-86-0100, 46 pp., http://www.dtic.mil/dtic/tr/fulltext/u2/a175173.pdf.

Arora, V. K., and Coauthors, 2011: Carbon emission limits required to satisfy future representative concentration pathways of greenhouse gases. *Geophys. Res. Lett.*, **38**, L05805, https://doi.org/10.1029/2010GL046270.

Bony, S., G. Bellon, D. Klocke, S. Sherwood, S. Fermepin, and S. Denvil, 2013: Robust direct effect of carbon dioxide on tropical circulation and regional precipitation. *Nat. Geosci.*, **6**, 447–451, https://doi.org/10.1038/ngeo1799.

Butler, A. H., D. W. J. Thompson, and R. Heikes, 2010: The steady-state atmospheric circulation response to climate change–like thermal forcings in a simple general circulation model. *J. Climate*, **23**, 3474–3496, https://doi.org/10.1175/2010JCLI3228.1.

Byrne, M. P., and T. Schneider, 2016a: Energetic constraints on the width of the intertropical convergence zone. *J. Climate*, **29**, 4709–4721, https://doi.org/10.1175/JCLI-D-15-0767.1.

——, and ——, 2016b: Narrowing of the ITCZ in a warming climate: Physical mechanisms. *Geophys. Res. Lett.*, **43**, 11 350–11 357, https://doi.org/10.1002/2016GL070396.

Collins, W. J., and Coauthors, 2011: Development and evaluation of an Earth-system model—HadGEM2. *Geosci. Model Dev.*, **4**, 1051–1075, https://doi.org/10.5194/gmd-4-1051-2011.

Cronin, T. W., 2014: On the choice of average solar zenith angle. *J. Atmos. Sci.*, **71**, 2994–3003, https://doi.org/10.1175/JAS-D-13-0392.1.

Davis, N. A., and T. Birner, 2013: Seasonal to multidecadal variability of the width of the tropical belt. *J. Geophys. Res. Atmos.*, **118**, 7773–7787, https://doi.org/10.1002/jgrd.50610.

Dufresne, J.-L., and Coauthors, 2013: Climate change projections using the IPSL-CM5 Earth System Model: From CMIP3 to CMIP5. *Climate Dyn.*, **40**, 2123–2165, https://doi.org/10.1007/s00382-012-1636-1.

Dunne, J. P., and Coauthors, 2012: GFDL's ESM2 global coupled climate–carbon Earth System Models. Part I: Physical formulation and baseline simulation characteristics. *J. Climate*, **25**, 6646–6665, https://doi.org/10.1175/JCLI-D-11-00560.1.

Emanuel, K. A., J. D. Neelin, and C. S. Bretherton, 1994: On large-scale circulations in convecting atmospheres. *Quart. J. Roy. Meteor. Soc.*, **120**, 1111–1143, https://doi.org/10.1002/qj.49712051902.

Gaetani, M., C. Flamant, S. Bastin, S. Janicot, C. Lavaysse, F. Hourdin, P. Braconnot, and S. Bony, 2017: West African monsoon dynamics and precipitation: The competition between global SST warming and CO_2 increase in CMIP5 idealized simulations. *Climate Dyn.*, **48**, 1353–1373, https://doi.org/10.1007/s00382-016-3146-z.

Giorgetta, M. A., and Coauthors, 2013: Climate and carbon cycle changes from 1850 to 2100 in MPI-ESM simulations for the Coupled Model Intercomparison Project phase 5. *J. Adv. Model. Earth Syst.*, **5**, 572–597, https://doi.org/10.1002/jame.20038.

Haywood, J. M., and Coauthors, 2016: The impact of equilibrating hemispheric albedos on tropical performance in the HadGEM2-ES coupled climate model. *Geophys. Res. Lett.*, **43**, 395–403, https://doi.org/10.1002/2015GL066903.

He, J., and B. J. Soden, 2015: Anthropogenic weakening of the tropical circulation: The relative roles of direct CO_2 forcing and sea surface temperature change. *J. Climate*, **28**, 8728–8742, https://doi.org/10.1175/JCLI-D-15-0205.1.

Held, I. M., and B. J. Soden, 2006: Robust responses of the hydrological cycle to global warming. *J. Climate*, **19**, 5686–5699, https://doi.org/10.1175/JCLI3990.1.

Iacono, M. J., J. S. Delamere, E. J. Mlawer, M. W. Shephard, S. A. Clough, and W. D. Collins, 2008: Radiative forcing by long-lived greenhouse gases: Calculations with the AER radiative transfer models. *J. Geophys. Res.*, **113**, D13103, https://doi.org/10.1029/2008JD009944.

Kamae, Y., M. Watanabe, M. Kimoto, and H. Shiogama, 2014: Summertime land–sea thermal contrast and atmospheric circulation over East Asia in a warming climate. Part II: Importance of CO_2-induced continental warming. *Climate Dyn.*, **43**, 2569–2583, https://doi.org/10.1007/s00382-014-2146-0.

Kociuba, G., and S. B. Power, 2015: Inability of CMIP5 models to simulate recent strengthening of the Walker circulation: Implications for projections. *J. Climate*, **28**, 20–35, https://doi.org/10.1175/JCLI-D-13-00752.1.

Lau, W. K. M., and K.-M. Kim, 2015: Robust Hadley circulation changes and increasing global dryness due to CO_2 warming from CMIP5 model projections. *Proc. Natl. Acad. Sci. USA*, **112**, 3630–3635, https://doi.org/10.1073/pnas.1418682112.

Li, X., and M. Ting, 2017: Understanding the Asian summer monsoon response to greenhouse warming: The relative roles of direct radiative forcing and sea surface temperature change. *Climate Dyn.*, **49**, 2863–2880, https://doi.org/10.1007/s00382-016-3470-3.

Long, M. C., K. Lindsay, S. Peacock, J. K. Moore, and S. C. Doney, 2013: Twentieth-century oceanic carbon uptake and storage in CESM1(BGC). *J. Climate*, **26**, 6775–6800, https://doi.org/10.1175/JCLI-D-12-00184.1.

Lu, J., G. Chen, and D. M. Frierson, 2008: Response of the zonal mean atmospheric circulation to El Niño versus global warming. *J. Climate*, **21**, 5835–5851, https://doi.org/10.1175/2008JCLI2200.1.

Ma, J., and S.-P. Xie, 2013: Regional patterns of sea surface temperature change: A source of uncertainty in future projections of precipitation and atmospheric circulation. *J. Climate*, **26**, 2482–2501, https://doi.org/10.1175/JCLI-D-12-00283.1.

Medeiros, B., B. Stevens, and S. Bony, 2015: Using aquaplanets to understand the robust responses of comprehensive climate models to forcing. *Climate Dyn.*, **44**, 1957–1977, https://doi.org/10.1007/s00382-014-2138-0.

Meehl, G. A., and Coauthors, 2012: Climate system response to external forcings and climate change projections in CCSM4. *J. Climate*, **25**, 3661–3683, https://doi.org/10.1175/JCLI-D-11-00240.1.

Merlis, T. M., 2015: Direct weakening of tropical circulations from masked CO_2 radiative forcing. *Proc. Natl. Acad. Sci. USA*, **112**, 13 167–13 171, https://doi.org/10.1073/pnas.1508268112.

Mlawer, E. J., S. J. Taubman, P. D. Brown, M. J. Iacono, and S. A. Clough, 1997: Radiative transfer for inhomogeneous atmospheres: RRTM, a validated correlated-k model for the longwave. *J. Geophys. Res.*, **102**, 16 663–16 682, https://doi.org/10.1029/97JD00237.

Phillips, N. A., 1956: The general circulation of the atmosphere: A numerical experiment. *Quart. J. Roy. Meteor. Soc.*, **82**, 123–164, https://doi.org/10.1002/qj.49708235202.

Pincus, R., and B. Stevens, 2013: Paths to accuracy for radiation parameterizations in atmospheric models. *J. Adv. Model. Earth Syst.*, **5**, 225–233, https://doi.org/10.1002/jame.20027.

——, and Coauthors, 2015: Radiative flux and forcing parameterization error in aerosol-free clear skies. *Geophys. Res. Lett.*, **42**, 5485–5492, https://doi.org/10.1002/2015GL064291.

Plesca, E., V. Grützun, and S. A. Buehler, 2018: How robust is the weakening of the Pacific Walker circulation in CMIP5 idealized transient climate simulations? *J. Climate*, **31**, 81–97, https://doi.org/10.1175/JCLI-D-17-0151.1.

Power, S. B., and G. Kociuba, 2011: What caused the observed twentieth-century weakening of the Walker circulation? *J. Climate*, **24**, 6501–6514, https://doi.org/10.1175/2011JCLI4101.1.

Rybka, H., and H. Tost, 2014: Uncertainties in future climate predictions due to convection parameterisations. *Atmos. Chem. Phys.*, **14**, 5561–5576, https://doi.org/10.5194/acp-14-5561-2014.

Shepherd, T. G., 2014: Atmospheric circulation as a source of uncertainty in climate change projections. *Nat. Geosci.*, **7**, 703–708, https://doi.org/10.1038/ngeo2253.

Stevens, B., and Coauthors, 2013: Atmospheric component of the MPI-M Earth System Model: ECHAM6. *J. Adv. Model. Earth Syst.*, **5**, 146–172, https://doi.org/10.1002/jame.20015.

Su, H., J. H. Jiang, C. Zhai, T. J. Shen, J. D. Neelin, G. L. Stephens, and Y. L. Yung, 2014: Weakening and strengthening structures in the Hadley circulation change under global warming and implications for cloud response and climate sensitivity. *J. Geophys. Res. Atmos.*, **119**, 5787–5805, https://doi.org/10.1002/2014JD021642.

Taylor, K. E., R. J. Stouffer, and G. A. Meehl, 2012: An overview of CMIP5 and the experiment design. *Bull. Amer. Meteor. Soc.*, **93**, 485–498, https://doi.org/10.1175/BAMS-D-11-00094.1.

Thompson, D. W., S. Bony, and Y. Li, 2017: Thermodynamic constraint on the depth of the global tropospheric circulation. *Proc. Natl. Acad. Sci. USA*, **114**, 8181–8186, https://doi.org/10.1073/pnas.1620493114.

Vecchi, G. A., and B. J. Soden, 2007: Global warming and the weakening of the tropical circulation. *J. Climate*, **20**, 4316–4340, https://doi.org/10.1175/JCLI4258.1.

Voldoire, A., and Coauthors, 2013: The CNRM-CM5.1 global climate model: Description and basic evaluation. *Climate Dyn.*, **40**, 2091–2121, https://doi.org/10.1007/s00382-011-1259-y.

Watanabe, M., and Coauthors, 2010: Improved climate simulation by MIROC5: Mean states, variability, and climate sensitivity. *J. Climate*, **23**, 6312–6335, https://doi.org/10.1175/2010JCLI3679.1.

Wing, A. A., K. A. Reed, M. Satoh, B. Stevens, S. Bony, and T. Ohno, 2018: Radiative–Convective Equilibrium Model Intercomparison Project. *Geosci. Model Dev.*, **11**, 793–813, https://doi.org/10.5194/gmd-11-793-2018.

Yukimoto, S., and Coauthors, 2012: A new global climate model of the Meteorological Research Institute: MRI-CGCM3—Model description and basic performance. *J. Meteor. Soc. Japan*, **90A**, 23–64, https://doi.org/10.2151/jmsj.2012-A02.

Zelinka, M. D., and D. L. Hartmann, 2010: Why is longwave cloud feedback positive? *J. Geophys. Res.*, **115**, D16117, https://doi.org/10.1029/2010JD013817.